AIAA AVIATION Forum
5-9 June 2017, Denver, Colorado
18th AIAA/ISSMO Multidisciplinary Analysis and Optimization Conference

10.2514/6.2017-4436

Aerostructural Optimization of the D8 Wing with Varying Cruise Mach Numbers

Charles A. Mader[*], Gaetan K. Kenway[†], J. R. R. A. Martins[‡]

University of Michigan, Department of Aerospace Engineering, Ann Arbor, MI

Alejandra Uranga[§]

University of Southern California, Dept. of Aerospace & Mechanical Eng., Los Angeles, CA

The D8 "double-bubble" is a new transport aircraft configuration proposed by MIT that has the potential to provide large improvements in fuel efficiency. It has been studied at the conceptual level and in low-speed wind tunnel tests, but there was, up to now, no higher fidelity transonic design. In this study, we use the conceptual design definition as a starting point and develop a high-fidelity aero-structural optimization problem for the D8 configuration using the MACH framework. Via gradient-based optimization techniques with coupled RANS and shell FEA, the D8 is optimized at three different cruise Mach numbers (0.72, 0.78, 0.84). The preliminary results presented confirm that the planforms designed with the conceptual level tools perform well and as predicted, and that some small improvements can be gained from further optimization. In spite of its limitations, this work confirms the viability of the D8 wing-body in the transonic regime and provides preliminary transonic geometries for future work.

I.   Introduction

A.   Background and Motivation

Global air traffic has increased by an average of over 5% annually over the last 5 years, an increase that is expected to continue for another 20 years [1, 2, 3]. With this growth and a continued industry focus on reducing emissions, operating cost and environmental impact, there is a strong desire to develop more efficient aircraft than those currently in the active fleet. Furthermore, while significant improvements in efficiency have been made over the last several decades, further improvement of the conventional tube-and-wing configuration has become increasingly challenging.

The NASA N+3 program seeks to develop aircraft technology concepts to provide 60% to 70% fuel burn reduction for an entry into service around 2030-2035. One of the concepts developed under this program is the MIT D8 "double-bubble" subsonic transport aircraft. Designed in the Boeing 737 or Airbus A320 class for a mission of 180 passengers and 3 000 nm range, it uses a lifting fuselage, low-sweep high-aspect ratio wings and boundary layer ingesting engines to achieve a significant reduction in fuel burn over a conventional aircraft. The D8 was studied at the conceptual level during the Phase 1 project [4, 5], and a low-speed (Mach 0.1) geometry was defined and tested in the NASA Langley 14- by 22-Foot Subsonic Tunnel during Phase 2 [6] which also included some complementary computational fluid dynamics (CFD) simulations [7]. However, a transonic geometry was still to be defined.

B.   Paper Scope

The present work is part of the N+3 Phase 3 project[a], whose goals included the design of a transonic D8 at a higher level of fidelity than the previous conceptual studies. Using the conceptual design definition as a starting point, we develop a high-fidelity, aero-structural optimization problem for the D8 configuration using the MACH framework developed by Kenway et al. [8]. It employs Reynolds-Averaged Navier–Stokes (RANS) CFD and shell finite element analysis (FEA) to compute accurate estimates of the aerodynamic and structural performance of the configuration. These estimates are then used to perform gradient-based aero-structural optimization. In addition to the wing-only

---

[*]Research Investigator, AIAA Senior Member
[†]Research Investigator, AIAA Senior Member
[‡]Professor, AIAA Associate Fellow
[§]Gabilan Assistant Professor, AIAA Senior Member
[a] carried out between 2015 and 2017 with MIT as the prime NASA contractor, under Cooperative Agreement NNX15AM91A

American Institute of Aeronautics and Astronautics

and wing-body-tail design at the D8's original cruise speed of Mach 0.72, we have completed wing-only and wing-body-tail designs at Mach 0.78 (a more standard cruise speed for commercial aircraft in the D8's class), as well as a wing-only design at the Mach 0.84 cruise speed typical of larger, longer-rage transports.

Presented next is the computational approach, including the initial geometry, the design calculations, and the optimization setup. The aero-structural optimization results are then presented for the wing-only cases, followed by the wing-body-tail designs. Finally, a summary and conclusions are provided.

II.   Approach

A.   Initial Geometry

The baseline D8 used for this study is the $M = 0.72$ TASOPT [9] conceptual design. The wing is defined as having a simple trapazoidal planform with an aspect ratio of 12.2, mid-chord sweep of 6.85 degrees, and a span of 118 ft. This span length is the maximum airport-allowed for an aircraft in the 737 or A320 class (FAA ADG III classification). The conceptual design also provided a basic structural layout, with a wingbox present from 15% chord to 65% chord.

By pairing this information with a set of supercritical airfoils, we generated the initial M=0.72 geometry shown in Figure 1. For the higher speed cases, also shown in Figure 1, the initial planform was modified in three ways:

1. The sweep was increased

2. The area was increased

3. A yehudi break was added to allow the trailing edge of the wing to stay perpendicular to the fuselage at the wing-body junction.

The initial geometric parameters for each of the configurations is summarized in Table 1.

Table 1. Initial geometry specifications; all cases have a structure encompassing 15-65% of the chord and a span of 118 ft.

Mach	Area (ft^2)	Mid-chord sweep (deg.)	Root chord (ft)	Break chord (ft)	Tip chord (ft)
0.72	1137	6.85	16.52	12.17	2.60
0.78	1279	24.00	24.38	12.89	2.79
0.84	1449	32.00	29.79	14.37	3.12

B.   Design Calculations

Since the N+3 goals are highly focused on reducing fuel burn, we use this as the objective function for these optimizations. This objective depends on three main characteristics of the aircraft, its aerodynamic performance, its weight and the performance of the engine. The details of each of these analyses are discussed in the following section.

1.   Weight and Balance

The weight of the aircraft is computed as the sum of a fixed weight (including payload, fuselage, tail, engine and miscellaneous components), a variable wing weight and a variable fuel weight. The fixed weights are taken from the TASOPT analysis of the aircraft as shown in Table 2. The wing weight is computed based on the wing box mass and an area based mass:

$$m_{\text{wing}} = m_{\text{wingbox}} C_w + m_{\text{area}} \frac{S}{S_{init}} \qquad (1)$$

The value of m_{area} is based on the weight of the non-structural wing components computed by TASOPT (flaps, slats, fixed leading edge, etc.), while the wing box factor C_w is calibrated by relating the weight of a structurally optimized wing box to the structural wing weight predicted by TASOPT.

The fuel weight is computed by rearranging the Breguet range equation:

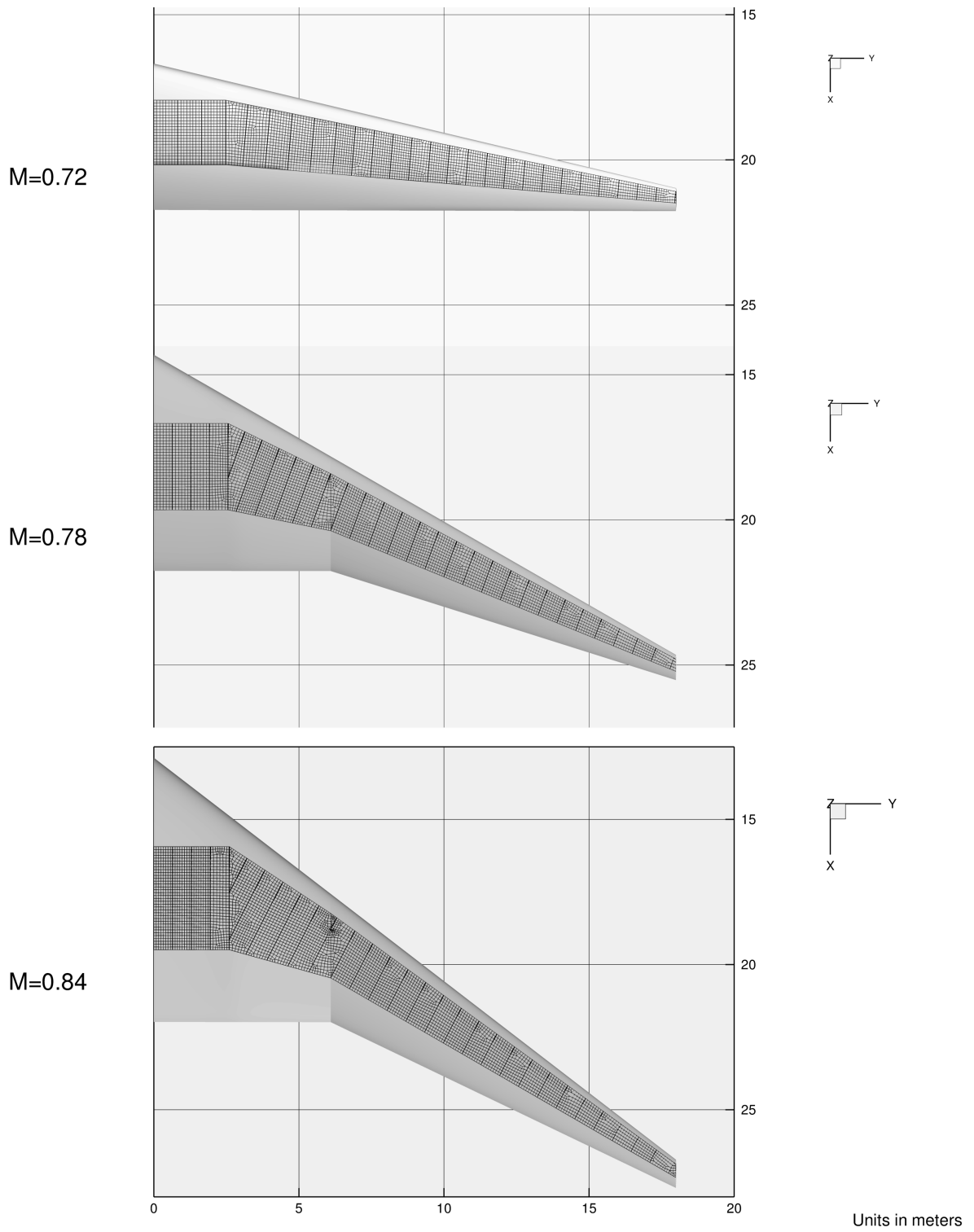$$R = \frac{V}{SFC} \frac{L}{D} \ln \frac{W_1}{W_2} \qquad (2)$$

American Institute of Aeronautics and Astronautics

M=0.72

M=0.78

M=0.84

Units in meters

Figure 1. Baseline planform and structural layout

Table 2. Reference weight breakdown (lb)

Component	M = 0.72	M = 0.78	M = 0.84
Payload	37 800	37 800	37 800
Fuselage	30 414	30 604	30 820
Tails	1 739	2 072	2 561
Engine	11 193	11 716	12 307
Other	5 861	6 053	6 291
Wing	12 994	14 996	17 295
Fuel	22 481	23 303	24 476
TOGW	123 378	127 440	132 445

to solve for the required fuel weight to acheive a fixed range. This gives a fuel burn equation of the following form:

$$W_1 = W_2 \exp\left(R \frac{SFC}{V} \frac{D}{L} \right). \tag{3}$$

For the aircraft in this study, we are using a range of 3000 nautical miles.

2. Engine Model

In order to simplify the analysis of the engine in this study, constant specific fuel consumption (SFC) values were assumed for each of the Mach numbers. This ignores the interactions between the engine and the aircraft drag and cruise altitude. However, in order to capture these trade-offs correctly, a full engine model is needed for each Mach number. That data was unavailable for this study, so the constant SFC values were considered to be more appropriate than an arbitrary engine model. The values of SFC used for this study, taken from the TASOPT analysis of each aircraft, are shown in Table 3.

Table 3. Specific fuel consumption values (lbm/lbf/hr)

Mach Number	SFC
0.72	0.45739
0.78	0.48250
0.84	0.50790

3. Aerodynamic Analysis

The aerodynamic analyses for this study were completed with ADflow. This is a cell-centered, multi-block/overset code that can solve either the Euler or RANS equations. The discretization is a second-order finite volume formulation with scalar, matrix and upwind dissipation schemes and multiple turbulence models. In this case we have used the RANS equations with scalar dissipation and the Spalart–Allmaras (SA) turbulence model.

Simulations in this study were completed on both wing-only and wing-body-tail geometries. For the wing-only geometry, corrections were included for the lift, drag, and moment of both the fuselage and the horizontal tail. These corrections are a function of the angle of attack and center of gravity location for both the fuselage and tail. The tail correction is also a function if the tail rotation angle. These corrections were computed using ADFlow on isolated fuselage and tail meshes and allow us to enforce the lift and trim constraints properly for the wing-only case. The

corrections take the general form show in Equation (4):

$$
\begin{aligned}
C_{L_{\text{Tail}}} &= C_{L_{\alpha_{\text{Tail}}}}(\theta_{\text{Tail}} + \alpha) + C_{L_{0_{\text{Tail}}}} \\
C_{D_{\text{Tail}}} &= A_{\text{Tail}}(\theta_{\text{Tail}} + \alpha)^2 + B_{\text{Tail}}(\theta_{\text{Tail}} + \alpha) + C_{\text{Tail}} \\
C_{m_{Tail}} &= C_{L_{\text{Tail}}}(x_{\text{ref}} - x_{\text{ref}_{\text{Tail}}}) + C_{m_{0_{\text{Tail}}}} \\
C_{L_{\text{Fuse}}} &= C_{L_{\alpha_{\text{Fuse}}}}\alpha + C_{L_{0_{\text{Fuse}}}} \\
C_{D_{\text{Fuse}}} &= A_{\text{Fuse}}\alpha^2 + B_{\text{Fuse}}\alpha + C_{\text{Fuse}} \\
C_{m_{Tail}} &= C_{L_{\text{Fuse}}}(x_{\text{ref}} - x_{\text{ref}_{\text{Fuse}}}) + C_{m_{0_{\text{Fuse}}}}
\end{aligned}
\tag{4}
$$

The coefficients for each of the cases are shown in Table 4. Additional constant drag corrections were also added for the vertical tail and for the estimated spurious drag as computed from the grid refinement study.

Table 4. Fuselage and tail correction coefficients

Coefficient	M = 0.72	M = 0.78	M = 0.84
$C_{L_{\alpha_{\text{Tail}}}}$	2.70×10^{-2}	2.40×10^{-2}	2.10×10^{-2}
$C_{L_{0_{\text{Tail}}}}$	5.70×10^{-2}	5.20×10^{-2}	5.30×10^{-2}
A_{Tail}	2.49×10^{-4}	2.84×10^{-4}	3.36×10^{-4}
B_{Tail}	1.41×10^{-3}	1.54×10^{-3}	2.03×10^{-3}
C_{Tail}	3.23×10^{-3}	3.31×10^{-3}	4.34×10^{-3}
$x_{\text{ref}_{\text{Tail}}}$	3.375×10^{1}	3.484×10^{1}	3.379×10^{1}
$C_{m_{0_{\text{Tail}}}}$	0.00×10^{0}	-2.30×10^{-1}	-2.20×10^{-1}
$C_{L_{\alpha_{\text{Fuse}}}}$	4.96×10^{-3}	4.18×10^{-3}	3.46×10^{-3}
$C_{L_{0_{\text{Fuse}}}}$	2.98×10^{-3}	3.33×10^{-3}	3.16×10^{-3}
A_{Fuse}	7.23×10^{-5}	7.95×10^{-5}	7.41×10^{-5}
B_{Fuse}	8.59×10^{-5}	1.26×10^{-4}	1.25×10^{-4}
C_{Fuse}	8.85×10^{-3}	1.03×10^{-2}	9.72×10^{-3}
$x_{\text{ref}_{\text{Fuse}}}$	-1.008×10^{1}	-1.101×10^{1}	-9.576×10^{0}
$C_{m_{0_{\text{Fuse}}}}$	5.28×10^{0}	6.00×10^{-2}	5.30×10^{-2}

Table 5. Mesh Sizes

Configuration		Fine (L0)	Medium Fine (L0.5)	Medium (L1)	Medium Coarse (L1.5)	Coarse (L2)
M = 0.72	Wing-only	16 662 528	N/A	2 082 816	N/A	260 352
	Wing-body-tail	76 146 432	21 582 624	9 518 304	2 680 160	1 189 788
M = 0.78	Wing-only	12 550 144	N/A	1 568 768	N/A	196 096
	Wing-body-tail	N/A	35 696 640	9 875 456	4 483 488	1 261 120
M = 0.84	Wing-only	12 550 144		1 568 768		196 096

4. Structural Analysis

The structural analysis is completed using the Toolkit for the Analysis of Composite Structures (TACS) [10]. This is a parallel finite element solver designed specifically for use in gradient-based optimization and includes native routines for computing single discipline and coupled aero-structural adjoint solutions. For this simulation we use shell finite elements that are equivalent to the CQUAD4 elements in NASTRAN. The shell element stiffness formulation

American Institute of Aeronautics and Astronautics

Table 6. Wing-body-tail, Trimmed aero-structural drag convergence at a fixed C_L of 0.5

Configuration	Extrapolated	Medium Fine (L0.5)	Medium (L1)	Medium Coarse (L1.5)	Coarse (L2)
M = 0.72	0.0248	-	0.0255	0.0264	0.0276
M = 0.78	0.0275	-	0.0279	0.0284	0.0290

is modified to calculate a smeared stiffness value assuming that there are blade stiffeners on the inside face of the structure. This approach allows us to compute and enforce local buckling constraints on the structure [11]. We also compute and constraint the von Mises stress on the structure, since we are modelling it as an aluminum structure (2024 grade). Specifically, we constrain the von Mises stress, multiplied by a safety factor of 1.5 to be less than or equal to the ultimate strength of the material.

5. Gust load factor

One of the structural load cases we consider is a gust load condition. This load case is generated by solving for the 1.0g aero-structural shape and then adding a load factor to the strains computed for this case to account for the increased load applied by the gust. The gust load factor is computed based on the FAR 23.341 gust load factor formula:

$$n = 1 + \frac{K_g U_{de} V C_{L_\alpha}}{498(W/S)} \qquad (5)$$

where n is the load factor, K_g is a load alleviation factor, U_{de} is the derived gust velocity, V is the aircraft velocity in knots, C_{L_α} is the aircraft lift curve slope (per radian) and W/S is the wing loading in psf. These quantities all vary throughout the Mach and altitude envelope of the aircraft. As a pre-processing step, we compute the gust load factor along the climb and cruise portion of the flight envelope. We then use the maximum load factor and its corresponding Mach number and altitude to generate the gust load case. The corresponding computations for the three configurations are shown in Figure 2. Note that the lift-curve slope increases with Mach number to a well defined peak in the transonic regime. Since the climb profile used here is a constant EAS climb, the Mach number increases with altitude, thus the lift-curve slope also increases with altitude to a similar well defined peak. It is this variation in the lift-curve slope that dominates the variation of the gust load factor. Therefore, the peak in the lift-curve slope also drives the peak in the gust load factor. Further, the Mach number that generates this peak is geometry dependent, so the maxium gust load factor is different for each of the three initial wing cases. In this particular case, the increased sweep of the higher speed wings has reduced the lift-curve slope, thereby reducing the maximum gust load factor for the higher speed cases. The exact Mach number, altitude and gust load factor for each of the three cases are summarized in Table 7. During the optimization, the load factor is adjusted to compensate for any changes in C_{L_α} that occur as the

Table 7. Gust Load Factors

Configuration	Initial Load Factor	Mach Number	Altitude (ft)
M = 0.72	2.41	0.725	23 889
M = 0.78	2.08	0.750	21 717
M = 0.84	2.00	0.758	18 676

wing design is changed. Note that in this computation, the M = 0.84 wing suffers from massive separation around 23,000 ft altitude which causes the steep drop off in C_{L_α} and load factor. This changes as the optimization progresses, but is compensated for by the dynamic computation of C_{L_α} included in the optimization problem.

6. Buffet separation constraint

We have also included a buffet onset constraint in the optimization. This constraint is based on the percentage of the wing area experiencing separated flow as determined by looking at the immediate off wall velocity. To apply
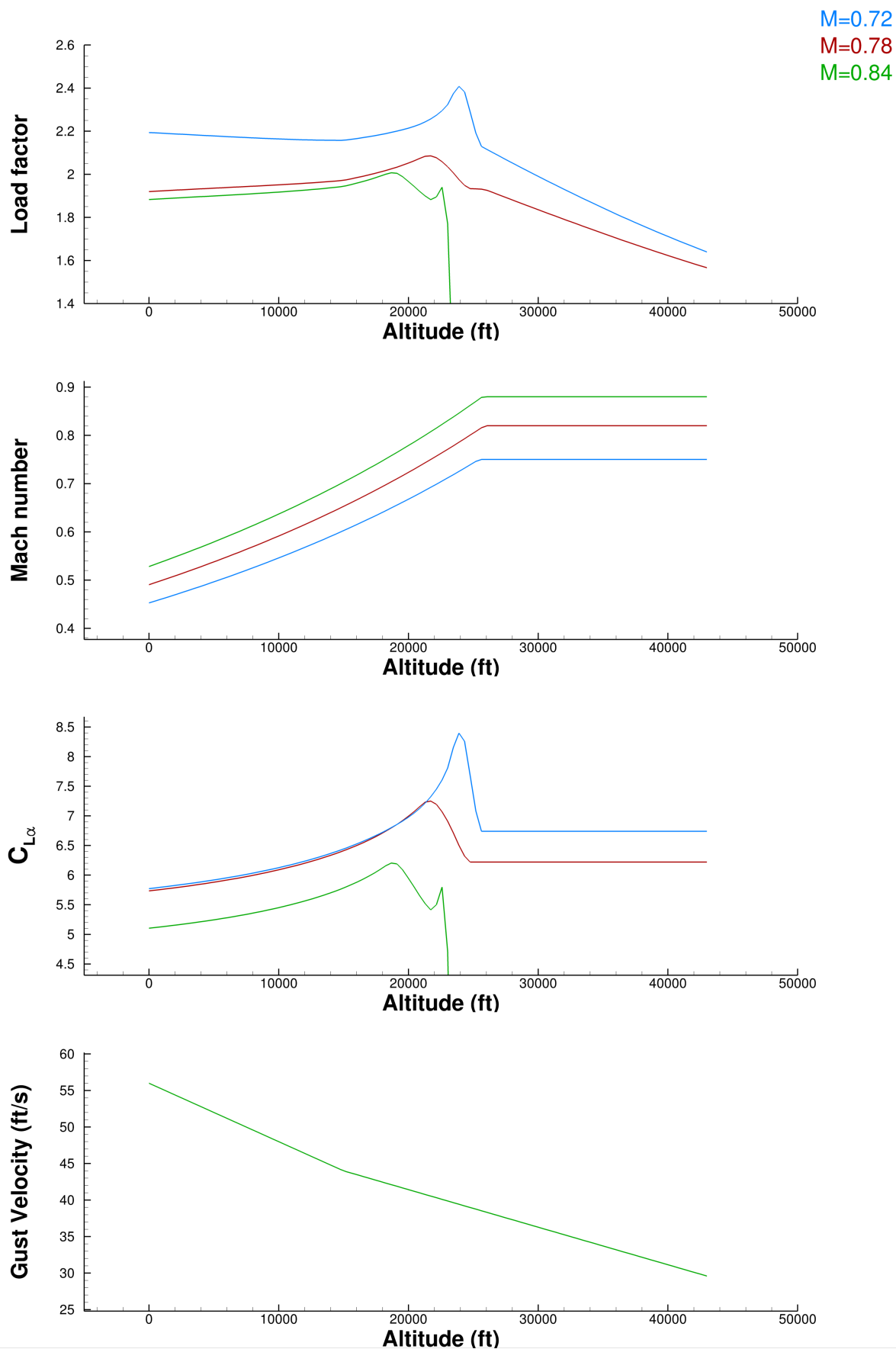
American Institute of Aeronautics and Astronautics

Figure 2. Gust load computations

American Institute of Aeronautics and Astronautics

this constraint, we include an additional high C_L point and an additional high Mach number point in the optimization formulation. These points are located to ensure that the design operating cruise point maintains a 1.3g margin to buffet. Full details on this paper can be found in Kenway and Martins [12].

The buffet onset constraint is of particular importance for the D8 design because of the high C_L and low sweep nature of the design. Both of these characteristics will limit the buffet margin, so it is important to ensure through the optimization that at least a 1.3g buffet onset margin is respected.

C.   Optimization Setup

We have completed optimizations of the D8 for both wing-only and wing-body-tail configurations. Both the wing-only and wing-body-tail configurations were optimized at M = 0.72 and M = 0.78, while just the wing-only case was optimized at M = 0.84. For each case, we have included eleven aero-structural analysis points in the optimization. The first five points form a Mach-C_L cross around the intended design point. The fuel burn performance of each of these points is included in the objective function with equal weighting. This ensures that the wing will perform well over a range of Mach numbers and lift coefficients. Points six and seven are the high C_L and high Mach number conditions used to evaluate the buffet onset constraint. The eighth point is evaluated at a fixed $\Delta\alpha$ from point number 1 to evaluate the C_{L_α} of the design. All eight of these cruise conditions are evaluated on the level 1 CFD mesh. The final three points are the maneuver conditions used to evaluate the von Mises stress and buckling constraints for the optimization. The first two points are evaluated at sea level with a velocity equal to $V_D = 1.2V_C$, while the third point is evaluated at the conditions corresponding to the maximum gust load as computed in Section 5. The loads for the maneuver cases are evaluated on the level 2 CFD mesh, as the accuracy of the drag is not important for these cases. However, the structural mesh used in these cases is more refined than the one used for the cruise cases, as the failure prediction is more important. Tables 8 through 10 summarize the points evaluated for each optimization case.

Table 8.   Aerostructural optimization analysis points: M = 0.72 case

Analysis points	M	Alt.(ft)	Load factor	Stress factor	Case
1	0.72	h	1.0g	-	Design point
2	0.73	h	1.0g	-	
3	0.71	h	1.0g	-	Multipoint
4	0.72	h + 2000	1.0g	-	cruise stencil
5	0.72	h − 2000	1.0g	-	
6	0.76	h	1.0g	-	Buffet
7	0.72	h + 2000	1.3g	-	conditions
8	0.72	h	1.0g	-	C_{L_α} comp. at $\Delta\alpha = 0.5$
M1	0.5446	0	2.5g	1.5	Pull-up
M2	0.5446	0	-1.0g	1.5	Push-over
M3	0.725	23889	1.0g	1.5×2.75	Gust

The full optimization formulation analyzed for this study is shown in Table 11. As we have mentioned above, the objective function is a weighted average of fuel burn. The geometric design variables include: chord, sweep, span and streamwise location for the wing as well as the rotation angle of the tail. Note that cases have been optimized with and without planform variables. Figure 3 shows the setup of the design variables for the M = 0.72 case. In addition to the geometric variables, we have the aerodynamic variable α, which combines with the tail rotation variable to satisfy the lift and trim constraints. We have also included several structural variables including: skin thickness, stiffener pitch, stiffener thickness and stiffener height.

In addition to the physical constraints on stress, buckling, lift, moment and separation, we have added some geometric constraints to the optimization formulation. These constraints include both volume constraints and thickness constraints. The volume constraints ensure that the volume inside the wing is physically large enough to hold the fuel and reserves required for the design mission. The thickness constraints are mainly in place to maintain a sensible geometry in areas where there is not enough physics in the model to prevent the optimizer from taking the geometry to extremes. The leading edge thickness constraint is required to keep a reasonable leading edge radius on the wing, since we are not analyzing any low speed, high lift cases, for which the leading edge shape is important. The trailing

Table 9. Aerostructural optimization analysis points: M = 0.78 case

Analysis points	M	Alt.(ft)	Load factor	Stress factor	Case
1	0.78	h	1.0g	-	Design point
2	0.79	h	1.0g	-	
3	0.77	h	1.0g	-	Multipoint
4	0.78	h + 2000	1.0g	-	cruise stencil
5	0.78	h − 2000	1.0g	-	
6	0.82	h	1.0g	-	Buffet
7	0.78	h + 2000	1.3g	-	conditions
8	0.78	h	1.0g	-	C_{L_α} comp. at $\Delta\alpha = 0.5$
M1	0.5896	0	2.5g	1.5	Pull-up
M2	0.5896	0	-1.0g	1.5	Push-over
M3	0.75	21717	1.0g	1.5×2.77	Gust

Table 10. Aerostructural optimization analysis points: M = 0.84 case

Analysis points	M	Alt.(ft)	Load factor	Stress factor	Case
1	0.84	h	1.0g	-	Design point
2	0.85	h	1.0g	-	
3	0.83	h	1.0g	-	Multipoint
4	0.84	h + 2000	1.0g	-	cruise stencil
5	0.84	h − 2000	1.0g	-	
6	0.88	h	1.0g	-	Buffet
7	0.84	h + 2000	1.3g	-	conditions
8	0.84	h	1.0g	-	C_{L_α} comp. at $\Delta\alpha = 0.5$
M1	0.6349	0	2.5g	1.5	Pull-up
M2	0.6349	0	-1.0g	1.5	Push-over
M3	0.758	18676	1.0g	1.5×2.87	Gust

edge thickness constraint is required to prevent trailing edge crossover, which is not physically possible. We have also included an absolute thickness constraint at the trailing edge spar as the optimzer wants to thin this area to increase bend-twist coupling. The wing needs to have sufficient height in this area to accomodate actuators for trailing edge devices, so we have imposed a seven centimetre minimum thickness in this area. Finally, in our early optimization solutions, the optimizer was collapsing the middle of the wing box at the tip of the wing, again to increase bend-twist coupling. Unfortunately, this produce unphysically thin section shapes at the wing tip. In order to counter this, we have added a thickness constraint from the yehudi break to the tip of the wing that limits the wing t/c to 75% of its initial value. A detailed view of these constraints is shown in Figure 4.

We have also included relative change constraints on the panels comprising the structure. In this case, no two adjacent structural panels may change in thickness more than a specified amount. This constraint is imposed to honor certain manufacturing limitations associated with wing construction. Finally, for the planform optimization case, we have included an overall span constraint. This constraint is based on the FAA class III span limit of 118 ft (36m) and is imposed on the projected span of the undeflected wing.
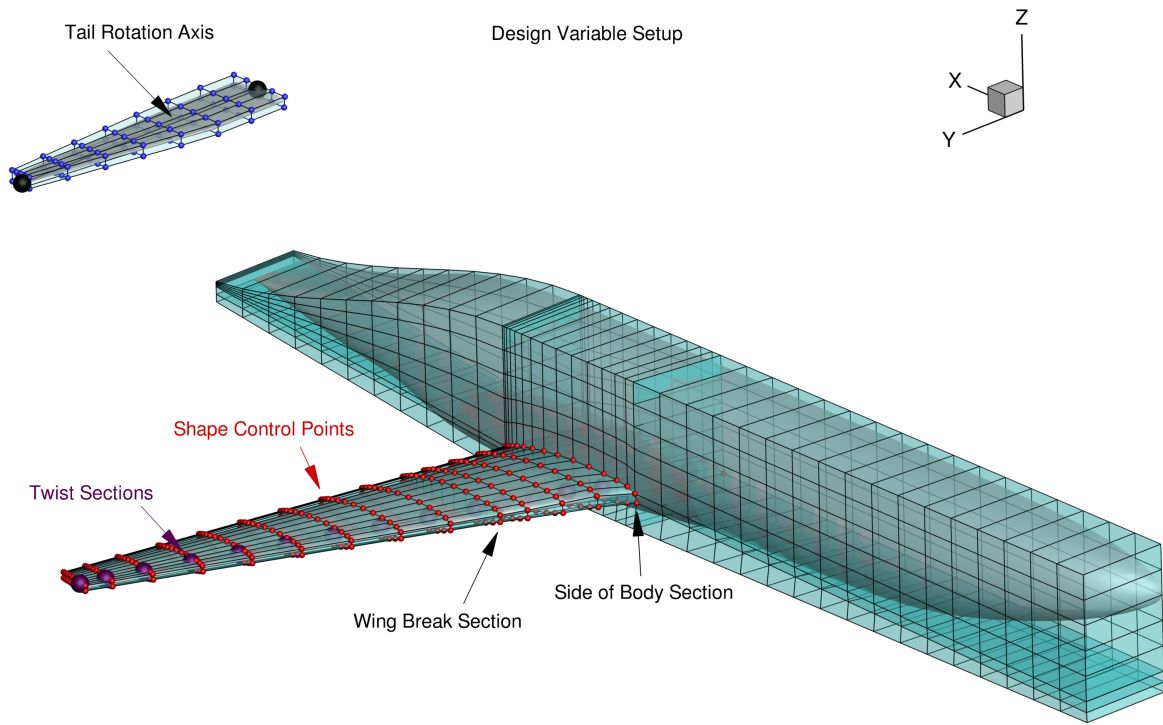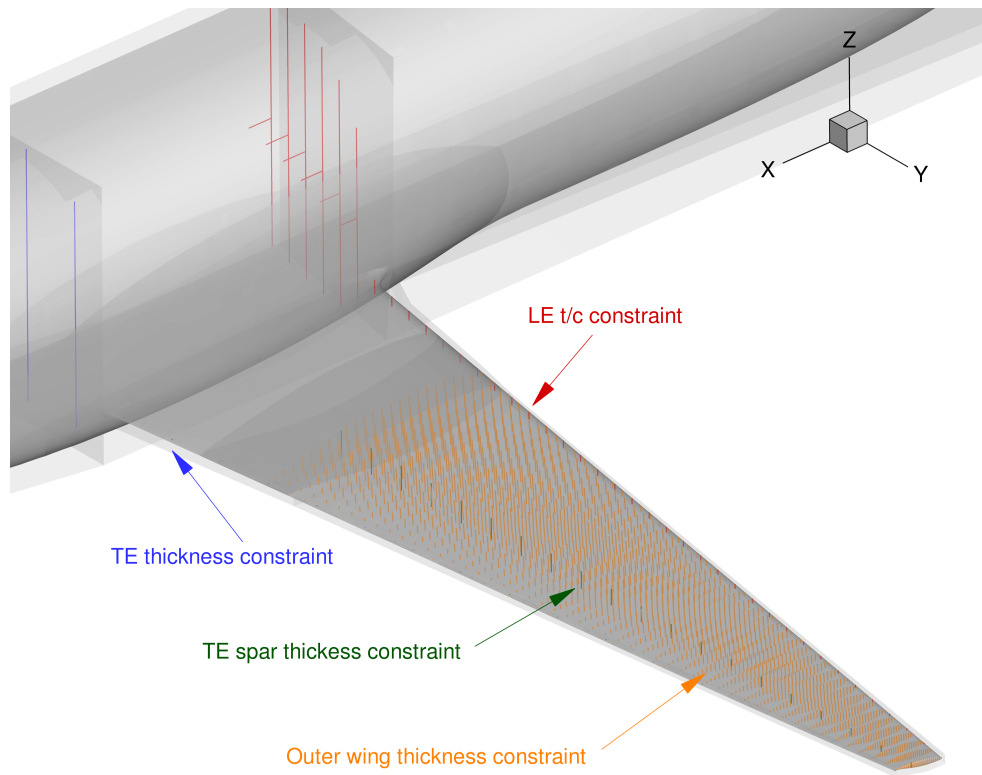
Design Variable Setup

Tail Rotation Axis

Shape Control Points

Twist Sections

Wing Break Section

Side of Body Section

Figure 3. Design variable setup

LE t/c constraint

TE thickness constraint

TE spar thickness constraint

Outer wing thickness constraint

Figure 4. Thickness constraint setup

Table 11. Aero-structural optimization formulation

	Function/variable	Description	Quantity
minimize	$\sum w_i F_{b_i}$	Fuel burn	5
with respect to	x_{twist}	Wing twist	14
	x_{airfoil}	FFD control points	450
	x^*_{planform}	Chord(3), sweep(1), span, wing location	6
	$x_{\text{alt.}}$	Cruise altitude	1
	x_{alpha_i}	Angle of attack at each flight condition	$7+3$
	$x_{\text{tail rot.}_i}$	Tail rotation angle at each condition	$7+3$
	$x_{\text{skin pitch}}$	Upper/lower stiffener pitch	2
	$x_{\text{spar pitch}}$	spar stiffener pitch	1
	$x_{\text{spar stiff height}}$	LE/TE spar stiffener height	58
	$x_{\text{rib stiffr pitch}}$	Stiffener pitch for ribs	31
	$x_{\text{rib stiffr height}}$	Stiffener height for ribs	31
	$x_{\text{panel thick}}$	Panel thickness skins/spars/ribs	149
	$x_{\text{stiff thick}}$	Panel stiffener thickness skins/spars/ribs	149
	$x_{\text{stiff height}}$	Panel stiffener height skins	116
subject to	$L = n_i W$	Lift constraint	$7+3$
	$C_m = 0$	Moment constraint	$7+3$
	$\text{Sep}_i \leq 0.04$	Separation constraint	$2+3$
	$b \leq 118$ ft	Gate constraint*	1
	$t_{\text{LE}}/t_{\text{LE}_{\text{Init}}} \geq 1.0$	Leading edge radius	40
	$t_{\text{TE}}/t_{\text{TE}_{\text{Init}}} \geq 1.0$	Trailing edge thickness	20
	$t_{\text{aftSpar}} \geq 0.07$	Aft spar height	20
	$t_{\text{Outer}}/t_{\text{Outer}_{\text{Init}}} \geq 0.75$	Outer wing thickness	1250
	$\mathcal{V}_{\text{wing}} > \mathcal{V}_{\text{fuel}}$	Minimum fuel volume	1
	$\text{KS}_{\text{buckling}} \leq 1$	2.5 g buckling	3
	$\text{KS}_{\text{vonMises}} \leq 1$	2.5 g yield stress	4
	$\text{KS}_{\text{buckling}} \leq 1$	1.0 g gust buckling	3
	$\text{KS}_{\text{vonMises}} \leq 1$	1.0 g gust yield stress	4
	$\text{KS}_{\text{buckling}} \leq 1$	-1.0 g buckling	3
	$\left\| x_{\text{panel thick}_i} - x_{\text{panel thick}_{i+1}} \right\| \leq 0.001$	Skin thickness adjacency	112
	$\left\| x_{\text{stiff thick}_i} - x_{\text{stiff thick}_{i+1}} \right\| \leq 0.001$	Stiffener thickness adjacency	112
	$\left\| x_{\text{stiff height}_i} - x_{\text{stiff height}_{i+1}} \right\| \leq 0.001$	Stiffener height adjacency	112
	$x_{\text{stiff thick}} - x_{\text{panel thick}} < 0.001$	Maximum stiffener-skin difference	158

* - For planform optimization cases only

III.   Results

Two sets of results are presented below. The first set of results are from the wing-only optimizations. These results explore the effect of various planform variables on the performance of the wing, though the structure and section shapes are also modified. The second set of results are from the combined wing-body-tail optimizations. These results focus on tuning the final shape of the wing for a fixed planform.

A.   Wing-Only Aero-structural Results

The results of the wing only optimizations for M = 0.72, M = 0.78 and M = 0.84 are shown in Figures 5 through 8. The main purpose of this set of optimizations is to refine the initial planform definitions of each design. Each optimization is run with the full optimization formulation described in Table 11 in order to maintain consistency with the final wing-body-tail optimization.

1.   M = 0.72 Case

As we can see from Figure 5, we have achieved a significant improvement in fuel burn with the optimized wing for the M = 0.72 case. The fuel burn reduction is 1514 lbs or 7% of the initial fuel burn relative to the initial planform. That said, there is relatively little change in the wing planform or spanwise thickness distribution. This indicates that the original planform of the wing was well designed by the conceptual level tools. One area of significant change is the spanwise lift distribution. The lift distribution is shifted significantly outboard relative to the initial design. This improves the L/D at the cost of a heavier wing, a result that is reflected in the wing weight and L/D numbers in the figure. A full summary of data for this case is present in Table 12

Another lift distribution that deserves some discussion is the -1.0g lift distribution on the initial design. This primarily comes from the asymmetry of the airfoils. When producing negative lift in the pushover case, the transonic foils become reflex airfoils and the aft portion of the foils, particularly near the root produce significant amounts of adverse lift. This causes most of the net lift to be cancelled out near the root of the wing, forcing the middle portion of the span to generate most of the lift. This is exacerbated by region of separated flow near the tip that affects the lift generated on the outboard portion of the wing. The reduction in washout evident in the optimized design as well as the small modifications in the section shapes are sufficient to alleviate this issue and generate a much more elliptical lift distribution for the optimized case. That said, the airfoil sections did not change significantly relative to their initial shapes. This indicates that overall, the initial design of the wing from the conceptual design tool was near optimal. Note that the original airfoil profiles were designed using multipoint optimization and inverse design using MSES and LINDOP. The multipoint optimization problem was setup to minimize average drag at a specified C_l much as described by Drela [13].

This optimization has also allowed us to develop a much more detailed description of the structural wing box, including stringer geometry and spacing, skin thickness and spar thickness. The initial and optimized wing-box can also be seen in Figure 5. The wing box is constrained to have zero displacement at the root and zero vertical displacement at the top of the rib at the side-of-body location. This configuration of constraints causes the highest skin thickness to be at the side-of-body location rather than at the wing root, since the side-of-body displacement constraint provides bending moment relief for the center wing box. Outboard of this location, we see a fairly typical decrease in skin thickness with span. In addition, the optimized wing box has larger top skin stringer spacing than the initial wing box, which indicates that the optimized wing has created slightly less buckling load on the upper wing surface. Note that this wing box layout is then used as the starting point for the full wing-body-tail optimization run in the next phase of the project.
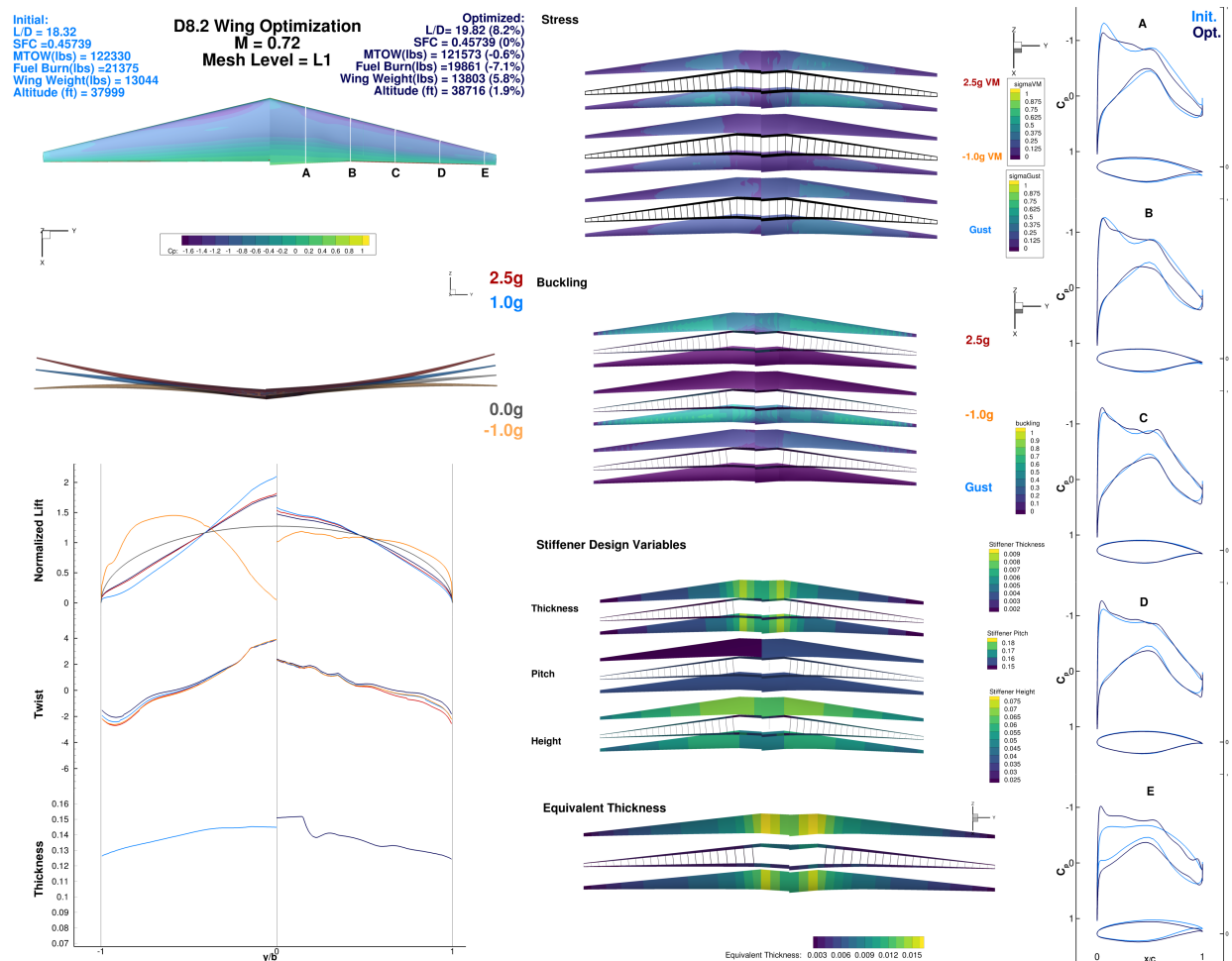
Figure 5. Wing aero-structural shape optimization: M = 0.72

Table 12. Wing aero-structural optimization Data: M = 0.72

Parameter	TASOPT	Initial Point	Optimized
TOGW (lbs)	123378	122330	121573
Wing weight (lbs)	12994	13044	13803
Fuel weight (lbs)	22481	21375	19861
L/D	18.689	18.32	19.82
Altitude (ft)	38000	37999	38716
TSFC (lbs/lbs/hr)	0.45739	0.45739	0.45739
$M^2 C_L$	0.3514	0.3284	0.3379
$C_L^2 S / \pi b^2$	0.0119	0.0104	0.0110

American Institute of Aeronautics and Astronautics

2. M = 0.78 Case

The improvement in the performance of the M = 0.78 wing-only optimization is even more significant than the previous case. In this instance, we achieved a reduction of 5619 lb or 20.8% of the initial fuel burn. We re-use the airfoils from the M = 0.72 case, so the airfoil shapes are not as well optimized for the flight condition as they were previously. This leads to significantly worse aerodynamic performance at the initial point than we had for the M = 0.72 case. As a result, there is a significant change in the C_p profiles during the optimization process. In this case, there is also a significant reduction in the t/c of the wing in the optimized result. The reduction of the t/c improves the aerodynamic performance of the wing at the expense of a higher wing weight. We again see the shift in the lift distribution to a more elliptically shaped distribution. This also improves the aerodynamic performance at the expense of structural weight, indicating that for this choice of objective function, the aerodynamic performance is more important that the structural weight. A full summary of the M = 0.78 data is shown in Table 13.

One very interesting result of this optimization is that despite the poor initial performance, the optimized planform is essentially the same as the initial planform. Given the poor initial performance, one might expect a more significant change. However, with the t/c and airfoil shapes optimized, the planform predicted from the simple conceptual methods turns out to be near optimal. Note that this is not simply because the optimizer is unable to move from its starting point. Figure 6 shows the sweep and span history from the optimization. In this history, we can see that the tip is swept back by 1.5m and the span is reduced by 1m in the first few iterations of the optimization. The optimization then works the planform back to the initial sweep and span over the coarse of the remaining iterations. This is a clear indication that the sweep and span of the initial planform are essentially optimal.
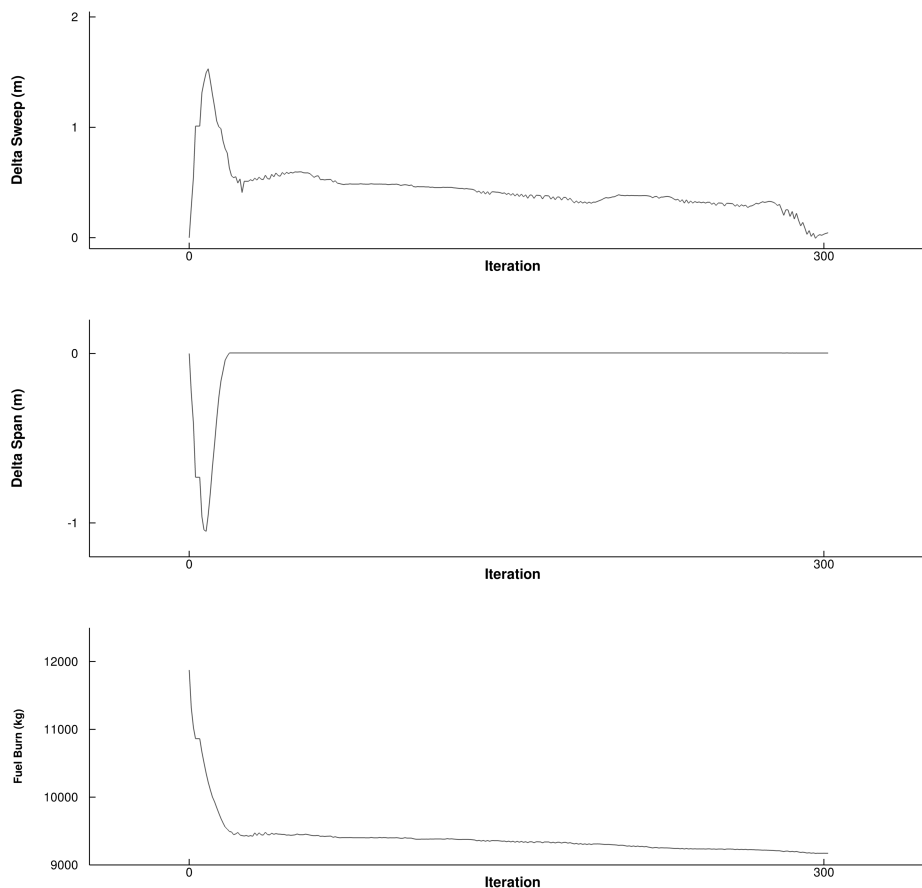

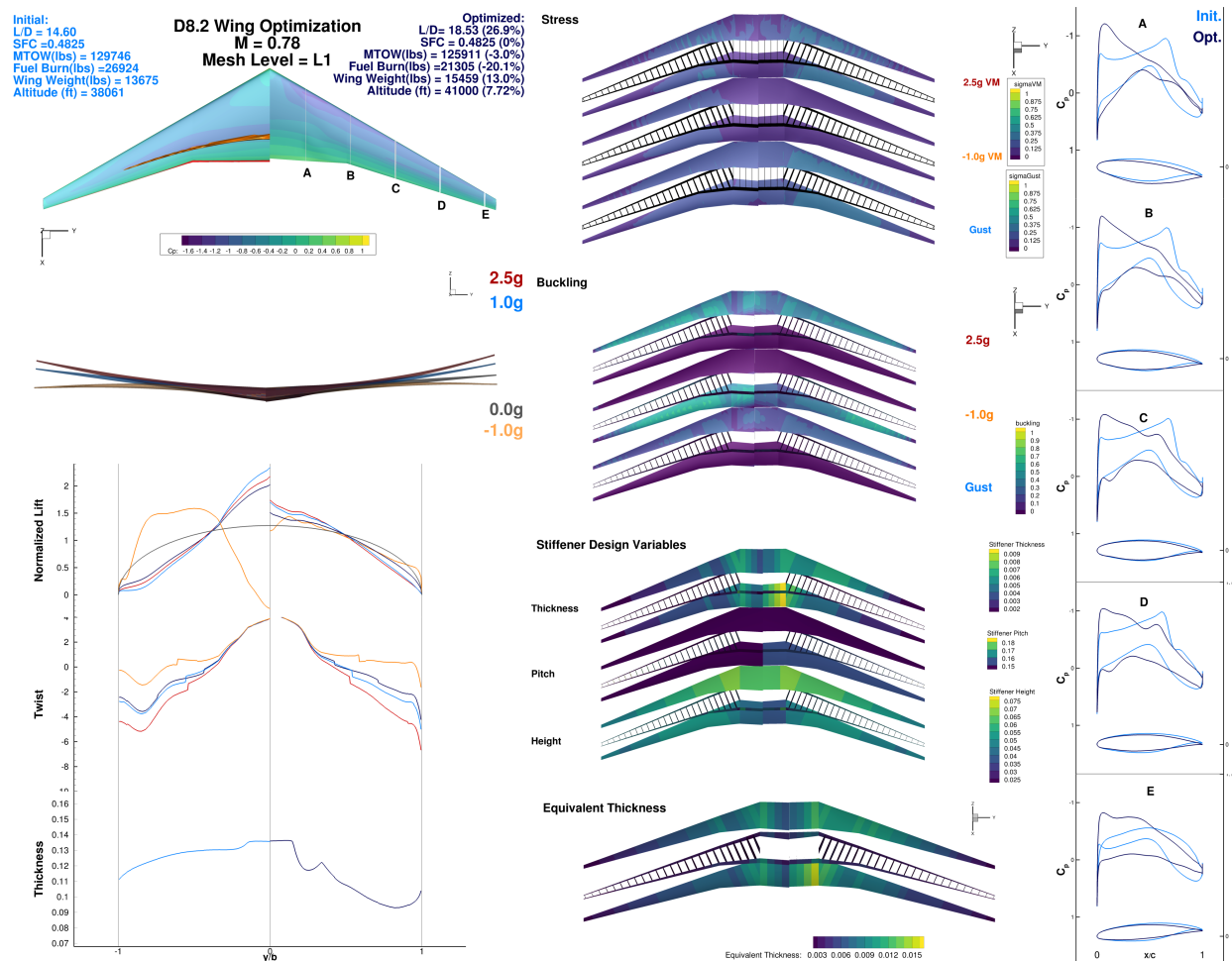**Figure 6. Search history of the M = 0.78 wing-only optimization**

American Institute of Aeronautics and Astronautics

Figure 7. Wing aero-structural shape optimization: M = 0.78

Table 13. Wing aero-structural optimization data: M = 0.78

Parameter	TASOPT	Initial Point	Optimized
TOGW (lbs)	127440	129746	125911
Wing weight (lbs)	14996	13675	15459
Fuel weight (lbs)	23303	26924	21305
L/D	18.24	14.60	18.53
Altitude (ft)	40240	38061	41000
TSFC (lbs/lbs/hr)	0.48246	0.48246	0.48246
$M^2 C_L$	0.3576	0.3023	0.3472
$C_L^2 S / \pi b^2$	0.0101	0.0072	0.0095

American Institute of Aeronautics and Astronautics

3.   M = 0.84 Case

The optimized M = 0.84 design also shows significant improvement over the initial design, with a 37.7% reduction in fuel burn and a 58% improvement in L/D. This improvement is again due the relatively poor starting point. While the sweep of the planform is designed for M = 0.84 the airfoils are again those from the M = 0.72 design, which results in the strong shock and large amount of separation on the initial design. In this case, the optimizer has made some meaningful changes to the planform of the wing. The sweep of the wing has been increased by approximately 2 degrees. Also, the tip chord has been reduced significantly, to only 66% of its initial size. These planform changes, along with the reduction in t/c and minor modifications to the airfoils allow for the elimination of the shock and the resulting trailing edge separation at the nominal cruise condition. Interestingly, the lift distribution in this case has stayed much more triangular than the previous two cases. This likely results from a lower percentage of the total drag coming from induced drag, making and elliptical lift distribution less important for this case. Note that because of the relatively large sweep angle present in the planform, there is a significant amount of bend-twist coupling in the wing. This allows for passive load alleviation at the maneuver conditions and helps to offset the weight penalty associated with the extra structural length of the highly swept wing.

From a structural perspective, we have similar trends to the previous two cases. The thickest part of the wing skin as at the side of body location. This is consistent with that location supporting the highest bending moment in the structure. The failure criteria are dominated by the buckling conditions as well as the gust case rather than the 2.5g maneuver. This leads is again driven by the high sweep on the wing, which allows a significant amount of passive load alleviation at the 2.5g maneuver condition. A full summary of the performance of the M = 0.84 design is shown in Table 14.
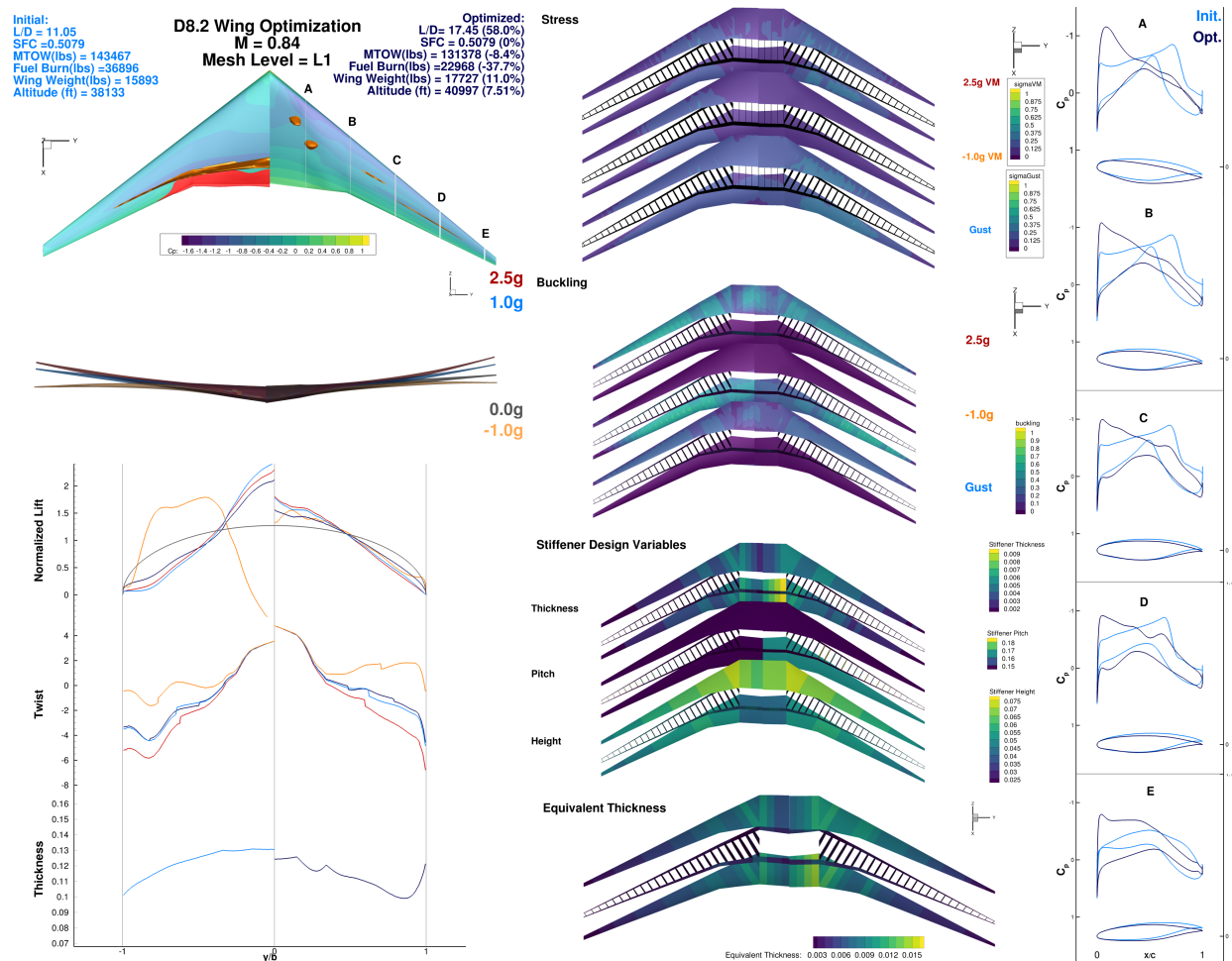
American Institute of Aeronautics and Astronautics

Figure 8. Wing aero-structural shape optimization: M = 0.84

Table 14. Wing aero-structural optimization Data: M = 0.84

Parameter	TASOPT	Initial Point	Optimized
TOGW (lbs)	132445	143468	131378
Wing weight (lbs)	17295	15895	17727
Fuel weight (lbs)	24476	36896	22968
L/D	17.73	11.05	17.45
Altitude (ft)	42215	38135	40997
TSFC (lbs/lbs/hr)	0.5079	0.5079	0.5079
$M^2 C_L$	0.3596	0.2873	0.3160
$C_L^2 S / \pi b^2$	0.0086	0.0055	0.0067

American Institute of Aeronautics and Astronautics

B. Wing-Body-Tail Aero-Structural Results

With the wing-only optimizations completed, we reconstructed the full wing-body-tail geometries with the optimized wing shapes. These geometries were then used to complete a second round of aero-structural optimizations using the same optimization formulation as the wing-only case, with the exception that the planform and wing locations have been fixed. These optimizations allow us to fine tune the wing section shapes in the presence of the fuselage. Note that neither the detailed shaping of the fuselage, nor shaping of the wing-body faring has been included in this optimization. This is beyond the capability of our current optimization framework.

1. $M = 0.72$ Case

The results of the combined wing-body-tail optimizations for $M = 0.72$ are shown in Figure 9. Now that we have the full configuration included in the analysis, we have eliminated the additional lift, drag and moment corrections for the fuselage and tail. We have retained a fixed drag mark up to account for the missing vertical tails and nacelle, but these components are not directly involved in the current aero-structural analysis so the impact of this approximation on the final result will be minimal. The fuel burn improvement from this optimization is not as significant as the improvement produced in the wing-only optimization at only 1% of the total fuel burn. However, there is still a significant change in the geometry in the optimized result. In this case, the t/c of the wing is reduced and the airfoil shapes are modified to reduce shocks. There is a slight shifting of the lift distribution to optimize the aero-structural trade-off between weight and drag.

The major benefit of the optimization is shown in Figure 10. This figure shows the contour of estimated fuel burn for a 3000 nm mission, for a given Mach number and C_L. In addition we have plotted the analyzed cruise points in black as well as the two analyzed buffet points in red. The red line represents a prediction of where the buffet onset will occur, while the green line represents a 1.3g margin on that buffet onset. Therefore, only the region below the green line is actually available for normal operations. The points in grey for the initial planform represent the original target C_L and Mach number for the D8 design. As we can see from this plot, that places the five point cruise stencil well outside of the feasible operating region. Even if we reduce the target operating C_L as shown with the black stencil, the high speed buffet point is still in-feasible. Looking at the contour of the optimized aircraft, we can see that the new geometry has allowed the contour to extend to include both buffet points. In addition, the entire cruise stencil is now inside the feasible operating region. Also, the feasible C_L for the operating region has been increased relative to the initial point. This allows the optimized design to operate at an altitude of 37600 ft, which is a much better operating ceiling than the 34500 ft available with the initial design.

2. $M = 0.78$ Case

The results of the combined wing-body-tail optimizations for $M = 0.78$ are shown in Figure 11. In this case, the performance increase relative to the baseline design is significant, a fuel burn reduction of approximately 6800 lbs or 27% of the initial fuel burn. This is relative to the initial un-optimized design, so the relative increase is larger than it would be relative to a more refined starting point. That said, there is a significant reduction in the t/c of the wing as well as significant change in the airfoil shapes and sectional C_p. Most of the improvement in the design is aerodynamic. The L/D has improved from 14.5 to 20, while the wing weight is only changed by 3%.

The change of performance in this case is easy to visualize using the fuel burn contours shown in Figure 12. The feasible operating region for the initial design is very limited. The required C_L to meet the 1.3g buffet margin is under 0.4 and the maximum operating Mach number is well below the target of $M = 0.82$ from the high speed buffet onset constraint.

After the optimization, the feasible operating region is well aligned with the high performance region of the aircraft. We can also see that the C_L at the design point has increase to approximately 0.55, which is right in the typical range for a transport aircraft. Further, the high performance region now is now aligned with the expected operating region of the aircraft, so the average fuel burn over the region of interest has decreased by over 3500 lbs.

3.   Limitations and Future Work

There are three main areas where the results presented in this report could benefit from additional investigation. The first limitation is the wing tip thickness constraint discussed above. A better solution to the issue of the optimizer collapsing the wing box at the wing tip would be to include additional load cases (such as a roll moment load case to check for aileron reversal) or an additional physical model such as flutter to accurately capture the reasons for that geometry being inappropriate. With this additional information available to the optimizer that thickness constraint could be removed and it is possible that the wing could end up thinner and lighter, particularly for the $M = 0.72$ case.
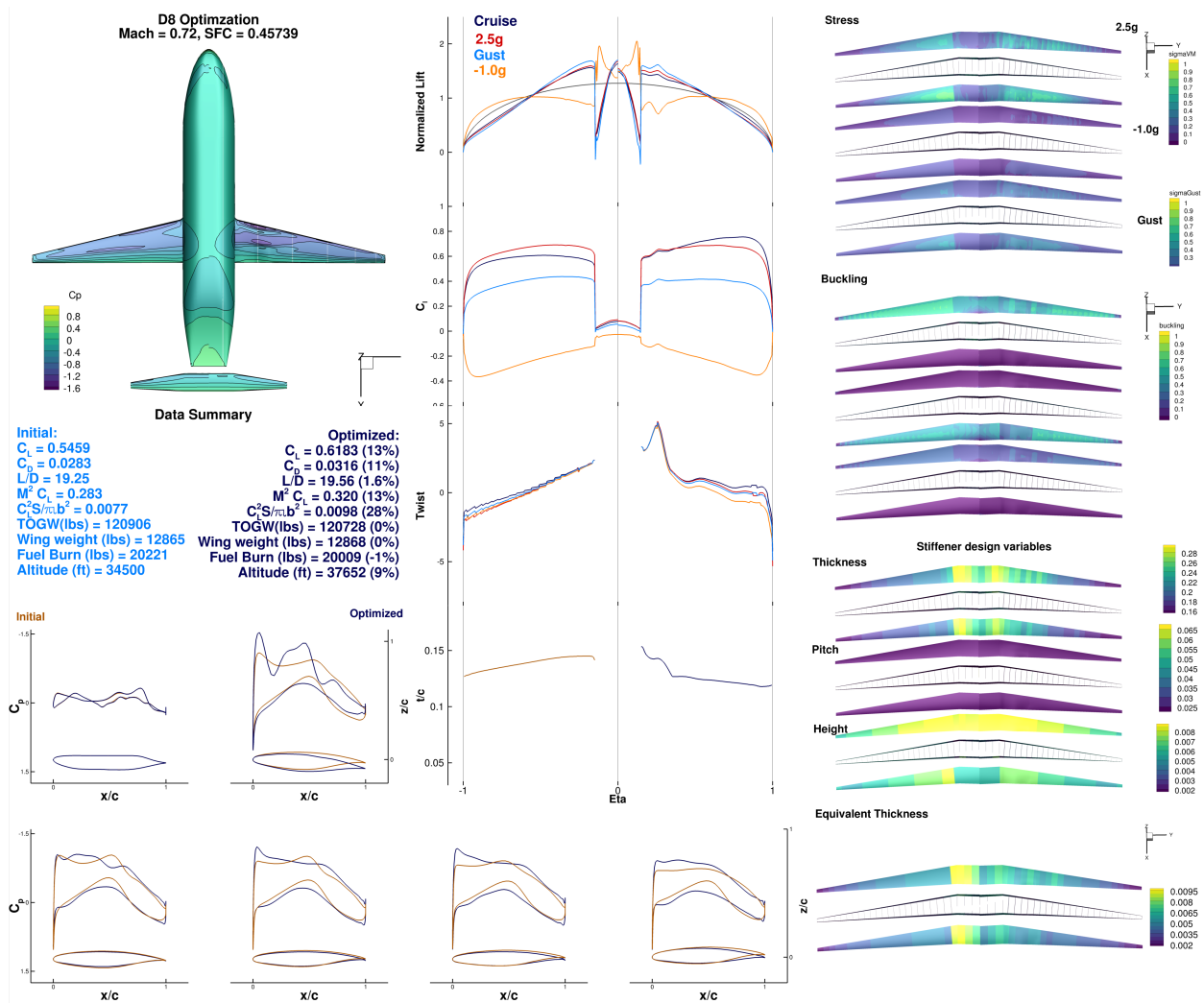
American Institute of Aeronautics and Astronautics

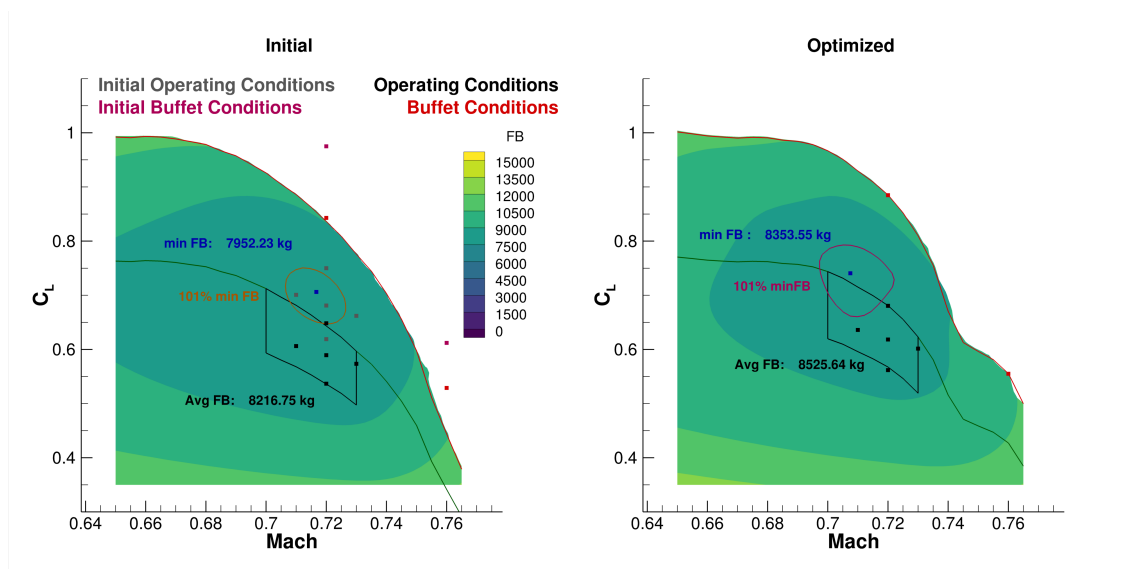**Figure 9. M = 0.72 optimized design**

Figure 10.   M = 0.72 configuration performance contours
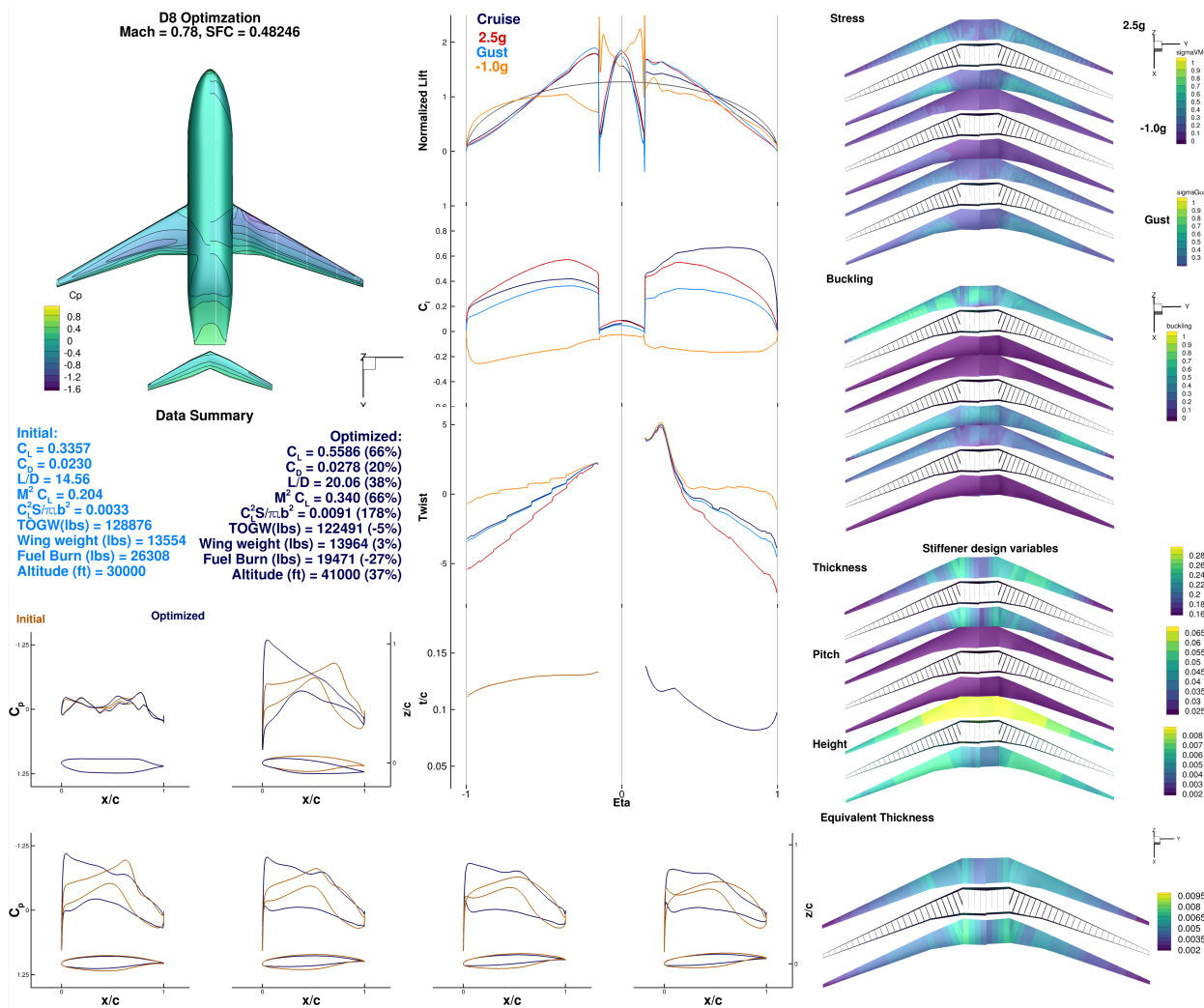
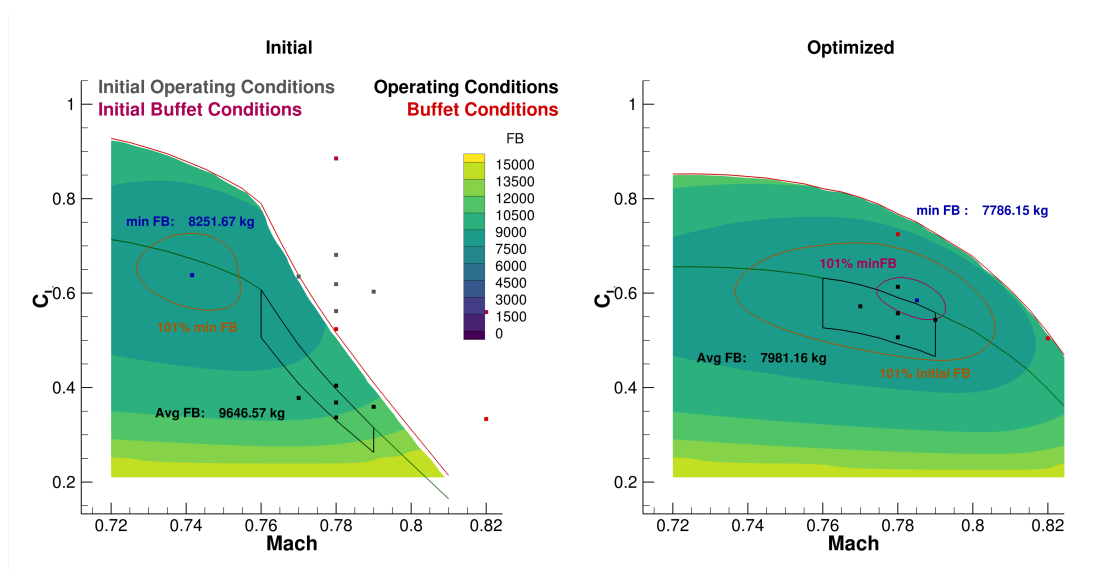**Figure 11.   M = 0.78 optimized design**

Figure 12.   M = 0.78 configuration performance contours

American Institute of Aeronautics and Astronautics

A second item deserving additional investigation is the relative mounting angle of the wing on the fuselage. The optimization process is modifying the lift distribution on the wing as well as the relative distribution of lift between the wing and fuselage. However, in the current setup, the wing-fuselage intersection line is fixed throughout the optimization. That means that the overall relative angle of the wing relative to the fuselage is unable to change and is therefore likely sub-optimal. A simple sweep over possible wing mounting angles would be a useful starting point, but ideally this degree of freedom would be included in the optimization.

Finally, the wing in this study was assumed to be essentially planar. The exploration of wing tip devices was left out of the design space entirely. The configuration considered here is the span constrained version of the D8. Since we know that the span constraint is active, and the optimized design flies at a relatively high C_L, it is likely that the optimizer would want to extend the wing vertically with a winglet to reduce the induced drag for the fixed span.

IV. Conclusion

The transonic design of the D8 subsonic transport aircraft has been evaluated using high-fidelity aero-structural optimization methods. Wing-alone designs have been evaluated and optimized for three cruise Mach numbers (M = 0.72, 0.78, and 0.84), and full wing-body-tail configurations have been evaluated and optimized for M = 0.72 and 0.78. The M = 0.72 and 0.78 cases confirmed that the planforms designed with the conceptual level tools performed well and as originally predicted. Modifications to the airfoil shapes, twist and t/c produced performance as good as or better than the performance predicted in the conceptual studies.

The results presented here are preliminary, and further refinements to the methodology are needed. In spite of its limitations, this work confirms the viability of the D8 wing-body-tail in the transonic regime and provides preliminary transonic geometries for future study and optimization. Using this same high-fidelity framework, optimization work on the aft-end, propulsor-airframe integration design of the D8 will be the subject of a future publication.

Acknowledgements

References

[1] "FAA Aerospace Forecast Fiscal Years 2016-2036," Federal Aviation Administration, 2016.

[2] "Boeing Current Market Outlook 2016-2035," Boeing, 2016.

[3] "Global Market Forecast 2016-2035," Airbus, 2016.

[4] Greitzer, E. M., Bonnefoy, P. A., de la Rosa Blanco, E., Dorbian, C. S., Drela, M., Hall, D. K., Hansman, R. J., Hileman, J. I., Liebeck, R. H., Lovegren, J., Mody, P., Pertuze, J. A., Sato, S., Spakovszky, Z. S., Tan, C. S., Hollman, J. S., Duda, J. E., Fitzgerald, N., Houghton, J., Kerrebrock, J. L., Kiwada, G. F., Kordonowy, D., Parrish, J. C., Tylko, J., Wen, E. A., and Lord, W. K., "N+3 Aircraft Concept Designs and Trade Studies, Volume 1," Final Report NASA/CR-2010-216794/VOL1, NASA Glenn Research Center, Cleveland, OH, 2010.

[5] Drela, M., "Development of the D8 Transport Configuration," *29th AIAA Applied Aerodynamics Conference*, American Institute of Aeronautics and Astronautics (AIAA), jun 2011. doi:10.2514/6.2011-3970.

[6] Uranga, A., Drela, M., Greitzer, E., Titchener, N., Lieu, M., Siu, N., Huang, A., Gatlin, G. M., and Hannon, J., "Preliminary Experimental Assessment of the Boundary Layer Ingestion Benefit for the D8 Aircraft," *52nd Aerospace Sciences Meeting*, American Institute of Aeronautics and Astronautics (AIAA), jan 2014. doi:10.2514/6.2014-0906.

[7] Pandaya, S., Huang, A., Espitia, A., and Uranga, A., "Computational Assessment of the Boundary Layer Ingesting Nacelle Desing of the D8 Aircraft," *52nd AIAA Aerospace Sciences Meeting, National Harbor, Maryland*, 2014.

[8] Kenway, G. K. W., Kennedy, G. J., and Martins, J. R. R. A., "Scalable Parallel Approach for High-Fidelity Steady-State Aeroelastic Analysis and Derivative Computations," *AIAA Journal*, Vol. 52, No. 5, May 2014, pp. 935–951. doi:10.2514/1.J052255.

[9] Greitzer, E. M., Bonnefoy, P. A., de la Rosa Blanco, E., Dorbian, C. S., Drela, M., Hall, D. K., Hansman, R. J., Hileman, J. I., Liebeck, R. H., Lovegren, J., Mody, P., Pertuze, J. A., Sato, S., Spakovszky, Z. S., Tan, C. S., Hollman, J. S., Duda, J. E., Fitzgerald, N., Houghton, J., Kerrebrock, J. L., Kiwada, G. F., Kordonowy, D., Parrish, J. C., Tylko, J., Wen, E. A., and Lord, W. K., "N+3 Aircraft Concept Designs and Trade Studies, Volume 2," Final Report NASA/CR-2010-216794/VOL2, NASA Glenn Research Center, Cleveland, OH, 2010.

[10] Kennedy, G. J. and Martins, J. R. R. A., "A Parallel Finite-Element Framework for Large-Scale Gradient-Based Design Optimization of High-Performance Structures," *Finite Elements in Analysis and Design*, Vol. 87, September 2014, pp. 56–73. doi:10.1016/j.finel.2014.04.011.

[11] Kennedy, G. J., Kenway, G. K. W., and Martins, J. R. R. A., "High Aspect Ratio Wing Design: Optimal Aerostructural Tradeoffs for the Next Generation of Materials," *Proceedings of the AIAA Science and Technology Forum and Exposition (SciTech)*, National Harbor, MD, January 2014. doi:10.2514/6.2014-0596.

[12] Kenway, G. K. W. and Martins, J. R. R. A., "Buffet Onset Constraint Formulation for Aerodynamic Shape Optimization," *AIAA Journal*, 2017. doi:10.2514/1.J055172, (In press).

[13] Drela, M., *Frontiers of Computational Fluid Dynamics*, chap. Pros and Cons of Airfoil Optimization, World Scientific, November 1998, pp. 363–381. doi:10.1142/9789812815774_0019.